BL-16A/2025G087

Examining Emergent Magnetism in $La_{0.7}Sr_{0.3}MnO_3$—Bi_2Te_3 Heterostructures Using X-ray Magnetic Circular Dichroism

Damian BRZOZOWSKI[1], Egil TOKLE[1], Kaoruho SAKATA[2], Kenta AMEMIYA[2] and Ingrid HALLSTEINSEN[1,*]

[1] Department of Materials Science and Engineering, Norwegian University of Science and Technology, Høgskoleringen 1, 7034 Trondheim, Norway

[2] Photon Factory, Institute of Materials Structure Science, High Energy Research Organization, 1-1 Oho, Tsukuba, Ibaraki 305-0801, Japan

We report synchrotron-based X-ray absorption spectroscopy (XAS) and X-ray magnetic circular dichroism (XMCD) measurements of $La_{0.7}Sr_{0.3}MnO_3$—Bi_2Te_3 heterostructures. The aim of the experiment was to obtain element-specific information on the oxidation state and magnetic response of Mn and Te species in the oxide—chalcogenide system. Mn $L_{3,2}$-edge XMCD confirms robust ferromagnetic ordering of the Mn sublattice, while comparison with a single $La_{0.7}Sr_{0.3}MnO_3$ reference film reveals changes in the Mn absorption line shape, indicating a modified Mn electronic environment in the heterostructure. Te $M_{5,4}$-edge XAS shows contributions from both Bi_2Te_3-like and oxidized Te states, consistent with the surface sensitivity of total electron yield detection. In contrast, the Te XMCD signal is weak and cannot be assigned unambiguously to a genuine Te magnetic moment. Complementary magnetometry reveals unconventional self-crossing hysteresis in LSMO—BT heterostructures, absent in the standalone LSMO reference film. Overall, the results indicate interfacial chemical reconstruction dominated by changes in the Mn electronic structure, while any induced Te magnetic contribution remains below the reliable detection limit of the present measurements.

1 Introduction

Interfaces between magnetically ordered materials and topological insulators are of considerable interest for realizing emergent electronic and spintronic phenomena.[1-4] In magnetic topological systems, time-reversal symmetry breaking can open an exchange gap in the topological surface states, enabling effects such as the quantum anomalous Hall effect. However, robust topological transport is often limited by disorder, chemical inhomogeneity, and parasitic conduction channels. One strategy to reduce dopant-induced disorder is to use the magnetic proximity effect, where magnetism is introduced into a topological insulator through contact with an adjacent ferromagnetic layer rather than by magnetic doping.[5-9]

In this work, we investigated heterostructures composed of ferromagnetic $La_{0.7}Sr_{0.3}MnO_3$ (LSMO) and topological-insulator Bi_2Te_3 (BT). LSMO is a high Curie-temperature ferromagnetic oxide, while BT is a prototypical three-dimensional topological insulator.[10-13] Combining these materials offers a route toward oxide–chalcogenide hybrid systems in which interfacial magnetic coupling may be used to modify the electronic and magnetic properties of the topological layer. At the same time, such heterostructures are chemically and structurally challenging because of the dissimilar bonding, lattice symmetry, and growth requirements of oxide perovskites and chalcogenide compounds.

The aim of the synchrotron measurements was to obtain element-specific information on the chemical and magnetic state of these heterostructures. X-ray absorption spectroscopy (XAS) was used to probe the oxidation state and local electronic structure of manganese and tellurium species, while X-ray magnetic circular dichroism (XMCD) was used to test for element-resolved magnetic contributions at the Mn and Te absorption edges. These measurements form part of a broader ongoing study comparing direct-growth LSMO—BT and seed-layer-mediated LSMO—Te—BT heterostructures using complementary probes, including polarized neutron reflectometry. In the present report, we focus on the direct-growth stack, presenting XAS/XMCD results, with magnetometry included as supporting characterization.

2 Experiment

LSMO—BT heterostructures were grown on (111)-oriented $SrTiO_3$ substrates (Shinkosha) via Pulsed Laser Deposition (PLD). The substrates were cleaned in sonication baths of acetone, ethanol and deionized water for 5 minutes each, followed by etching in a buffered

hydrofluoric acid solution (1:9 volumetric ratio of HF and NH_4F) for 45 seconds to ensure single termination of the surface and annealing at 1050 °C for 1 hour in O_2 flow to achieve a step-terrace topography.

Prior to installation on a sample holder, the substrates were rinsed in an ethanol bath. Once the substrate was installed in the PLD chamber, it was degassed through the annealing process at 400 °C for 1 hour at a base pressure of $5*10^{-8}$ mbar. A KrF excimer laser ($\lambda = 248$ nm) was used to deposit thin films. For LSMO, the substrate temperature T was set to 650 °C, and the chamber was filled with O_2 gas under the pressure p of 0.3 mbar. The laser pulsing frequency $\nu = 1$ Hz, and the laser fluence $f = 2.0$ J cm^{-2}. To minimize oxygen vacancies within the oxide structure, post-growth annealing was performed at 100 mbar O_2 for 1 hour. For BT thin films, the following growth conditions were selected: $T = 220$ °C, $p = 1.0$ mbar Ar, $\nu = 0.2$ Hz, $f = 0.5$ J cm^{-2}.

Element-resolved X-ray Magnetic Circular Dichroism (XMCD) measurements were performed on manganese $L_{3,2}$ edges and tellurium $M_{5,4}$ edges to investigate the presence of magnetic ordering within deposited layers. An incidence angle was set at 30° relative to the sample surface. Magnetic field $H = 0.7$ T was applied parallel to the X-ray beam. The presented data display an average of several measurements (between 4 and 16, depending on a sample), sorted by the polarization of light (left- and right-handed for the circular polarization). Presented measurements were performed using the total electron yield (TEY). The averaged spectra were divided by the I_0 beam channel, which is particularly important for analysis of the tellurium $M_{5,4}$ edges, which correspond to a similar photon energy range as the $L_{3,2}$ edges of chromium that is present within the optics of the beamline. All profiles were normalized to the maximum of the mean peak of an edge.

A series of magnetometry measurements was performed to characterize the net magnetic behavior of the samples. The measurements were performed using the Quantum Design Physical Property Measurements System (PPMS) in Vibrating Sample Magnetometer (VSM) mode. For comparison, additional field-dependent magnetization curves were collected on the single LSMO thin film and an LSMO—BT heterostructure with the thinner LSMO layer. Prior to each measurement, samples were warmed above their Curie temperature T_C, demagnetized using the oscillation mode, and cooled to the target temperature for field-dependent magnetization measurements. Each loop was acquired in the field range of ±0.5 T.

3 Results and Discussion

XAS and XMCD measurements were used to obtain element-specific information on the chemical and magnetic state of the LSMO—BT heterostructure. Particular attention was given to the Mn $L_{3,2}$ edges, which probe the electronic structure of the LSMO layer, and to the Te $M_{5,4}$ edges, which may reveal changes in the Bi_2Te_3-related region and possible proximity-induced magnetic contributions.

Fig. 1(a) shows the Mn $L_{3,2}$-edge XAS and XMCD spectra measured for the LSMO—BT heterostructure. The L_3 and L_2 edges correspond to $2p_{3/2} \rightarrow 3d$ and $2p_{1/2} \rightarrow 3d$ excitations, respectively. A clear dichroic signal is observed, confirming ferromagnetic ordering of Mn in the heterostructure. The XMCD amplitude reaches approximately 42% at a photon energy of 640.4 eV.

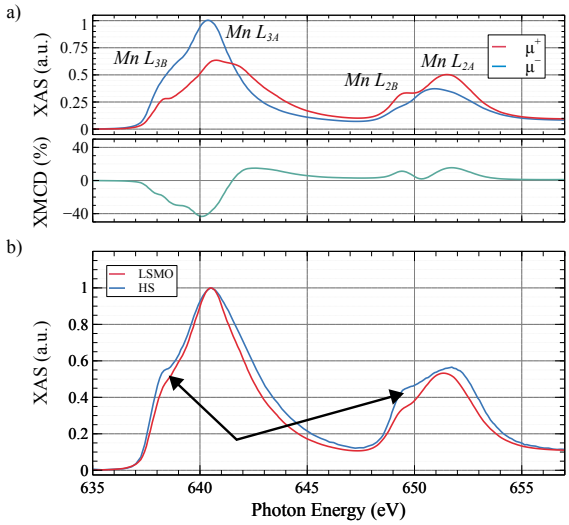

Fig. 1: X-ray absorption and dichroism spectra of the Mn $L_{3,2}$ edge. a) XAS and XMCD of the heterostructure. The dichroism intensity is expressed as a fraction of the XAS signal, normalized to the edge's maximum. b) Comparative XAS of the heterostructure and a single LSMO thin film. The plot inset shows the Mn L_2 edge.

To evaluate whether the Mn electronic structure is modified in the heterostructure, the Mn $L_{3,2}$-edge spectrum was compared with that of a single LSMO reference film, as shown in Fig. 1(b). The reference LSMO spectrum is consistent with the expected mixed Mn valence state of $La_{0.7}Sr_{0.3}MnO_3$.[14,15] In contrast, the LSMO—BT heterostructure exhibits additional spectral weight around 638 eV and 649 eV (marked with arrows), as well as changes on the high-energy side of the absorption edge. These features indicate that the Mn

electronic environment is altered in the heterostructure. The changes may reflect a modified Mn valence state, for example through a contribution from lower-valence Mn species, or interfacial chemical reconstruction involving Mn. The XAS results therefore suggest that the interface modifies the Mn oxidation state and local electronic structure compared with the single LSMO layer.

The Te $M_{5,4}$-edge spectra of the same sample are shown in Fig. 2. Compared with the Mn $L_{3,2}$ edges, the Te $M_{5,4}$ edges are weak relative to the background, making both XAS and XMCD analysis more challenging. The M_5 and M_4 edges correspond to $3d_{5/2} \rightarrow 5p$ and $3d_{3/2} \rightarrow 5p$ transitions, respectively. The spectra contain features at approximately 571.2 eV and 575.1 eV at the M_5 edge, and at 582.1 eV and 585.3 eV at the M_4 edge. The features near 571.2 eV and 582.1 eV are consistent with Te states expected for Bi_2Te_3, whereas the features near 575.1 eV and 585.3 eV resemble contributions from oxidized Te species, such as Te^{4+} in TeO_2. Since the spectra were acquired in total electron yield mode, which is surface sensitive, the signal likely contains contributions from both the Bi_2Te_3 layer and surface-oxidized Te. A weak contribution from Cr-related features in the beamline optics near this energy range cannot be fully excluded.

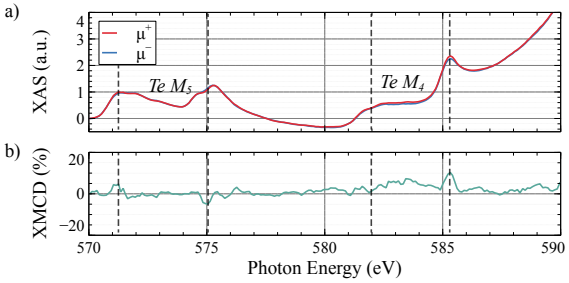

Fig. 2: a) X-ray absorption spectra of the Te $M_{5,4}$. b) The corresponding dichroism spectra.

The corresponding Te XMCD signal is shown in Fig. 2(b). A weak apparent dichroic contrast is observed near selected Te $M_{5,4}$-edge features, with an amplitude of approximately 5% near the M_5 region and up to approximately 10% near the feature at 585.3 eV. However, the Te absorption signal is weak relative to the background, and possible nonmagnetic contributions from surface oxidation, beamline-related background features, or normalization artifacts cannot be excluded. Therefore, the observed Te XMCD-like contrast should be treated with caution and cannot be assigned unambiguously to a genuine Te magnetic moment. The data do not provide conclusive evidence for proximity-induced magnetic polarization of Te, although they also do not rule out a weak magnetic proximity effect below the reliable detection limit of the present measurements.

Complementary magnetometry measurements were performed to assess whether the changes observed by XAS/XMCD are reflected in the macroscopic magnetic response. Fig. 3(a) shows *M(H)* hysteresis loops for the LSMO—BT heterostructure measured at 300 K and 110 K. At 300 K, the sample exhibits unconventional self-crossing hysteresis loop near zero field, while the high-field response remains characteristic of a ferromagnet. The saturation magnetization is approximately 1.34 μ_B/Mn. The loop is also weakly shifted along the applied-field axis by approximately -1.7 Oe.

At 110 K, the heterostructure shows more conventional ferromagnetic hysteresis, although a small horizontal loop shift remains. To test whether the anomalous loop shape is masked by the larger LSMO contribution at lower temperature, a heterostructure with a thinner, 20 nm LSMO layer was measured. As shown in Fig. 3(b), this sample retains self-crossing hysteresis at 110 K, with a loop shift of approximately -4 Oe and a saturation magnetization of approximately 3.52 μ_B/Mn. In contrast, the standalone LSMO reference film shown in Fig. 3(c) exhibits conventional ferromagnetic hysteresis without self-crossing behavior or a measurable horizontal shift.

These magnetometry results support that the unusual magnetic response is associated with the LSMO—BT heterostructure rather than with LSMO alone. While the macroscopic measurements do not identify the microscopic origin of this response, they are consistent with the Mn-edge XAS/XMCD results showing that the Mn electronic structure is modified in the heterostructure.

The XAS and XMCD results provide element-specific information on the chemical and magnetic state of the LSMO—BT heterostructure. At the Mn $L_{3,2}$ edges, the strong XMCD signal confirms that the Mn sublattice remains ferromagnetically ordered in the heterostructure. At the same time, comparison with a single LSMO reference film shows that the Mn absorption line shape is modified after deposition of the Bi_2Te_3-based layer. The additional spectral weight observed near the low-energy side of the Mn L_3 and L_2 edges suggests that part of the Mn environment differs from that of the reference LSMO layer. This may indicate a change in the local Mn valence state, possibly involving lower-valence Mn species, or the formation of a chemically reconstructed interfacial region. These observations are consistent with the expectation that the oxide—chalcogenide interface is chemically active. In

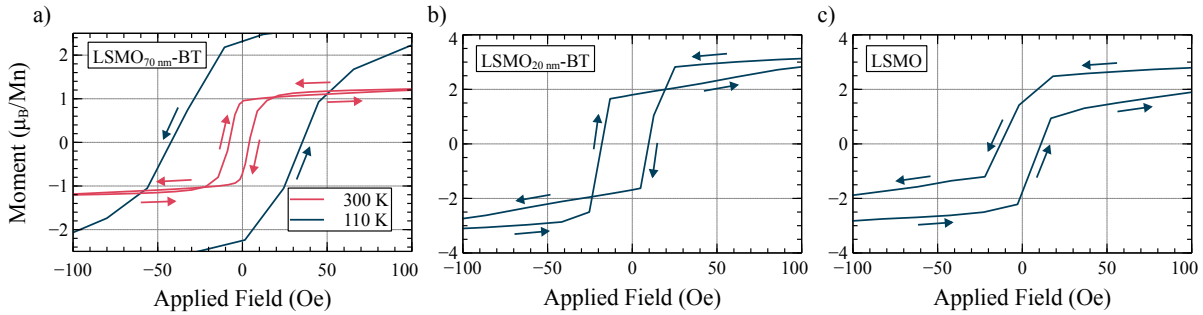

Fig. 3: a) Zoomed-in hysteresis loops around $H = \pm 100$ Oe. a) LSMO—BT heterostructures with the 70 nm thick LSMO layer. Scans collected at two temperatures are plotted to compare the magnetic response. b) Comparative heterostructure with the 20 nm thick LSMO layer. c) Single LSMO layer.

LSMO—BT heterostructures, Mn provides the magnetic sublattice of the ferromagnetic oxide, while Te is prone to diffusion, desorption, and oxidation. Interfacial reactions involving these elements could therefore modify both the chemical state and magnetic response of the system. The Mn-edge XAS results support this scenario by showing that the Mn electronic structure is not identical to that of the LSMO reference film.

The Te $M_{5,4}$-edge spectra indicate that more than one Te chemical environment contributes to the measured signal. Features assigned to Te in Bi_2Te_3 are observed together with additional features consistent with oxidized Te species. Because the spectra were measured in total electron yield mode, the surface sensitivity of the technique likely enhances the contribution from surface oxidation. Therefore, the Te XAS results suggest that the probed region contains both BT-like and oxidized Te components.

In contrast to the Mn edges, the Te XMCD response is weak and difficult to interpret. Although a small apparent dichroic signal is observed at selected Te-edge features, the weak absorption intensity, possible surface-oxidation contribution, and background-related artifacts prevent a definitive assignment to a genuine Te magnetic moment. The data therefore do not provide conclusive evidence for proximity-induced magnetic polarization of Te. However, this does not rule out a weak magnetic proximity effect in the BT-related layer, since the induced moment or exchange-related spectral contrast may be below the detection limit of the present measurements.[16,17]

Overall, the synchrotron results show that the LSMO—BT heterostructure exhibits robust Mn ferromagnetism together with a modified Mn electronic structure compared with single-layer LSMO. The Te XAS spectra reveal contributions from both Bi_2Te_3-like and oxidized Te states, while the Te XMCD data remain inconclusive. These findings indicate that interfacial chemical reconstruction plays an important role in the oxide—chalcogenide heterostructure, and that the dominant unambiguous magnetic signal detected by XMCD originates from Mn with an altered oxidation state.

Acknowledgement

D.B. acknowledges Takashi HONDA of the High Energy Accelerator Research Organization (Tsukuba, Japan) for his assistance in supplementary VSM magnetic characterization.

References

[1] C.-Z. Chang, J. Zhang, X. Feng, J. Shen, Z. Zhang, M. Guo, K. Li, Y. Ou, P. Wei, L.-L. Wang, et al., Science 340, 167 (2013).
[2] F. Katmis, V. Lauter, F. Nogueira, B. Assaf, M. Jamer, P. Wei, B. Satpati, J. Freeland, I. Eremin, D. Heiman, P. Jarillo-Herrero, and J. Moodera, Nature 533 (2016), 10.1038/nature17635.
[3] M. Li, Q. Song, W. Zhao, J. A. Garlow, T.-H. Liu, L. Wu, Y. Zhu, J. S. Moodera, M. H. W. Chan, G. Chen, and C.-Z. Chang, Phys. Rev. B 96, 201301 (2017).
[4] Y. Tokura, K. Yasuda, and A. Tsukazaki, Nature Reviews Physics 1, 126 (2019).
[5] L. Alegria, H. Ji, N. Yao, J. Clarke, R. J. Cava, and J. R. Petta, Applied Physics Letters 105 (2014), 10.1063/1.4892353.
[6] C. Tang, C.-Z. Chang, G. Zhao, Y. Liu, Z. Jiang, C.-X. Liu, M. R. McCartney, D. J. Smith, T. Chen, J. S. Moodera, et al., Science advances 3, e1700307 (2017).
[7] S. Zhu, G. Shi, P. Zhao, D. Meng, G. Liang, X. Zhai, Y. Lu, Y. Li, L. Chen, and K. Wu, Chinese Physics B 27, 076801 (2018).
[8] S. Zhu, D. Meng, G. Liang, G. Shi, P. Zhao, P. Cheng, Y. Li, X. Zhai, Y. Lu, L. Chen, and K. Wu, Nanoscale 10, 10041 (2018).
[9] L. Pan, A. Grutter, P. Zhang, X. Che, T. Nozaki, A. Stern, M. Street, B. Zhang, B. Casas, Q. L. He, et al., Advanced Materials 32, 2001460 (2020).
[10] Y. Tokura, JSAP Int 2, 12 (2000).

[11] M. Izumi, Y. Ogimoto, Y. Konishi, T. Manako, M. Kawasaki, and Y. Tokura, Materials Science and Engineering: B 84, 53 (2001).
[12] Y. Chen, J. G. Analytis, J.-H. Chu, Z. Liu, S.-K. Mo, X.-L. Qi, H. Zhang, D. Lu, X. Dai, Z. Fang, et al., science 325, 178 (2009).
[13] H. Zhang, C.-X. Liu, X.-L. Qi, X. Dai, Z. Fang, and S.-C. Zhang, Nature physics 5, 438 (2009).
[14] J. Kavich, M. Warusawithana, J. Freeland, P. Ryan, X. Zhai, R. Kodama, and J. Eckstein, Physical Review B—Condensed Matter and Materials Physics 76, 014410 (2007).
[15] I. Hallsteinsen, M. Moreau, A. Grutter, M. Nord, P. E. Vullum, D. A. Gilbert, T. Bolstad, J. Grepstad, R. Holmestad, S. Selbach, et al., Physical Review B 94, 201115 (2016).
[16] V. M. Pereira, C. N. Wu, K. Höfer, A. Choa, C. A. Knight, J. Swanson, C. Becker, A. C. Komarek, A. D. Rata, S. Rößler, S. Wirth, M. Guo, M. Hong, J. Kwo, L. H. Tjeng, and S. G. Altendorf, Physica Status Solidi (B) Basic Research 258 (2021), 10.1002/pssb.202000346.
[17] C.-Y. Yang, L. Pan, A. J. Grutter, H. Wang, X. Che, Q. L. He, Y. Wu, D. A. Gilbert, P. Shafer, E. Arenholz, et al., Science advances 6, eaaz8463 (2020).

* ingrid.g.hallsteinsen@ntnu.no